DRAFT VERSION DECEMBER 12, 2018
Typeset using LaTeX **twocolumn** style in AASTeX62

WASP-4b Arrived Early for the TESS Mission

L. G. BOUMA,[1] J. N. WINN,[1] J.-M. DÉSERT,[2] K. G. STASSUN,[3,4] T. DAYLAN,[5] M. HILL,[6] S. KANE,[6] G. R. RICKER,[5] R. VANDERSPEK,[5] D. W. LATHAM,[7] S. SEAGER,[8] J. M. JENKINS,[9] Z. BERTA-THOMPSON,[10] J. RODRIGUEZ,[11] K. COLÓN,[12] J. D. TWICKEN,[9,13] B. WOHLER,[9,13] D. A. CALDWELL,[9,13] POC1, POC2, AND POC3

[1] *Department of Astrophysical Sciences, Princeton University, 4 Ivy Lane, Princeton, NJ 08540, USA*
[2] *API, University of Amsterdam, P.O. Box 94249, 1090 GE Amsterdam, The Netherlands*
[3] *Vanderbilt University, Department of Physics & Astronomy, 6301 Stevenson Center Lane, Nashville, TN 37235, USA*
[4] *Fisk University, Department of Physics, 1000 17th Avenue N., Nashville, TN 37208, USA*
[5] *Department of Physics and Kavli Institute for Astrophysics and Space Research, Massachusetts Institute of Technology, Cambridge, MA 02139, USA*
[6] *Department of Earth Sciences, University of California, Riverside, CA 92521, USA*
[7] *Harvard-Smithsonian Center for Astrophysics, 60 Garden Street, Cambridge, MA 02138, USA*
[8] *Department of Earth, Atmospheric, and Planetary Sciences, Massachusetts Institute of Technology, Cambridge, MA 02139, USA*
[9] *NASA Ames Research Center, Moffett Field, CA 94035, USA*
[10] *Department of Astrophysical and Planetary Sciences, University of Colorado, Boulder, CO 80309, USA*
[11] *Harvard-Smithsonian Center for Astrophysics, 60 Garden Street, Cambridge, MA 02138, USA*
[12] *NASA Goddard Space Flight Center, Exoplanets and Stellar Astrophysics Laboratory (Code 667), Greenbelt, MD 20771, USA*
[13] *SETI Institute, Mountain View, CA 94043, USA*

(Received December 12, 2018; Revised —; Accepted —)

Submitted to AAS journals.

ABSTRACT

By combining data from the Transiting Exoplanet Survey Satellite (TESS) with data from previous studies, we show that the transit times of WASP-4b are incompatible with a constant orbital period. The transits observed by TESS occurred 77.8 ± 10.8 seconds earlier than one would expect, based on the previous data. The orbital period appears to be shrinking by $\dot{P} = -12.1 \pm 1.2$ milliseconds per year. A simple clock offset is unlikely, because TESS observations of other hot Jupiters (WASP-6b, 18b, and 46b) are compatible with a constant period and rule out a 77.8-second offset at the 6.3σ level. The timing variations seem to be astrophysical, and could be caused by apsidal precession, or perhaps by tidal decay. The latter seems implausible on theoretical grounds, as it would require a stellar quality factor $Q'_\star \approx 3 \times 10^4$. Apsidal precession would imply an eccentricity $e \approx 1.6 \times 10^{-3}$, and the possibility of measuring the planet's Love number. A Doppler shift from WASP-4's acceleration towards us could account for at most one quarter of the observed period change (at 2σ). Further observations are needed to confirm and understand the timing variation.

Keywords: planet-star interactions — planets and satellites: individual (WASP-4b, WASP-5b, WASP-6b, WASP-12b, WASP-18b, WASP-46b) — binaries: close

Corresponding author: L. G. Bouma
luke@astro.princeton.edu

1. INTRODUCTION

Long-term monitoring of hot Jupiter transit and occultation times should eventually reveal two distinct processes. First, whenever the summed spin and orbital angular momenta in a hot Jupiter system fall below a critical value, the system becomes unstable to tidal decay (Counselman 1973; Hut 1980). Most hot Jupiters satisfy this condition; their orbits should be shrinking (Levrard et al. 2009; Matsumura et al. 2010). The rate of decay is uncertain, and depends on how friction dissipates energy carried by gravitational tides (Ogilvie 2014 gives a review). If we could directly measure orbital decay rates, it would inform our understanding of tidal dissipation. This is important because the dissipation rates determine the fate of the system. During its inspiral, if the planet fills its Roche lobe below the stellar surface, the drag force from the stellar envelope accelerates the inspiral, leading to a 'direct-impact' merger (Metzger et al. 2012; MacLeod et al. 2018) Alternatively, if the planet fills its Roche lobe above above the stellar surface, then it could either be disrupted into an accretion disk or it could slowly transfer mass to the star (Metzger et al. 2012; Valsecchi et al. 2015; Jackson et al. 2016). Further afield, the outcome of the eventual interaction between the Earth and red giant Sun also hinges on the efficiency of tidal dissipation (Rasio et al. 1996).

The second process that long-term timing studies should reveal is apsidal precession, *i.e.*, rotation of the orbital ellipse within the orbital plane. Apsidal precession has been observed extensively in eclipsing binaries (*e.g.*, Schwarzschild 1958; Torres et al. 2010; Borkovits et al. 2015) and has been detected in a handful of exoplanet systems, including circumbinary planets (Kepler-413 Kostov et al. 2014; Kepler-453 Welsh et al. 2015, planets orbiting rapidly rotating stars (Kepler-13 Szabó et al. 2012, 2014, Masuda 2015; PTFO 8-8695 Barnes et al. 2013), and systems with multiple interacting giant planets (Kepler-108 Mills & Fabrycky 2017; Kepler-693 Masuda 2017). Apsidal precession is not regularly observed in hot Jupiter systems, perhaps in part because their orbits are nearly circular. However, there are many mechanisms that could pump hot Jupiter orbits away from circularity (see § 4.2, and Bailey & Goodman 2019), which would then lead to observable timing variations. For hot Jupiters, the apsidal precession is usually dominated by the quadrupolar distortion of the planet by the star's tidal force (Ragozzine & Wolf 2009). The observed precession rate in a hot Jupiter system could thus be used to compute the planet's Love number, giving a third parameter along with the mass and radius with which to describe the planet's interior structure (*e.g.*, Batygin et al. 2009, who performed a similar procedure for HAT-P-13b). Measuring small eccentricities and understanding their origin might also help us understand the dynamical histories and inflated radii of hot Jupiters. (*e.g.*, Dawson & Johnson 2018; Ibgui et al. 2010, respectively)

While numerous indirect studies have called attention to population-level effects of tidal decay (Jackson et al. 2009; Hansen 2010; Penev et al. 2012; Husnoo et al. 2012; Matsakos & Königl 2016; Collier Cameron & Jardine 2018; Penev et al. 2018), the most convincing direct evidence to date for either orbital decay or apsidal precession has come from WASP-12b. Maciejewski et al. (2016) showed that the transit times of WASP-12b did not follow a linear ephemeris at 5σ confidence, and measured $\dot{P} = -26 \pm 4\,\mathrm{ms\,yr^{-1}}$. Using new timing data, Patra et al. (2017) found $\dot{P} = -29 \pm 3\,\mathrm{ms\,yr^{-1}}$. If the period change were caused entirely by tidal decay, the implied modified stellar quality factor would be $Q'_\star \approx 2 \times 10^5$. Standard equilibrium tides do not predict this level of dissipation (Penev & Sasselov 2011; Ogilvie 2014). The needed level of friction might come from dynamical tides, or obliquity tides (Weinberg et al. 2017; Millholland & Laughlin 2018). The former is more likely if WASP-12 is a subgiant, but the observational constraints favor a main-sequence model (Bailey & Goodman 2019). More data are needed to understand the WASP-12b timing variations.

This work focuses on the hot Jupiter WASP-4b, which orbits its host star every 1.34 days, at a distance of $a/R_\star = 5.46$ (Wilson et al. 2008; Hoyer et al. 2013). WASP-4b is a plausible candidate for orbital decay, and has been observed often over the past decade. The host is a G7V dwarf, and is on the main sequence (§ 2.3). The orbit is consistent with being circular (but see § 4.2), and having sky-projected obliquity of zero (Triaud et al. 2010; Beerer et al. 2011; Sanchis-Ojeda et al. 2011).

We measure new transit times for WASP-4b using TESS lightcurves (§ 2.1, 2.2), and calculate the system's parameters empirically (§ 2.3). We merge the new times with previous observations and compare three models (§ 3): a constant period, a decaying period, and a slightly eccentric orbit undergoing precession. We rule out a constant period, but cannot firmly distinguish between the latter two possibilities. Each would have interesting implications (§ 4). We rule out the possibility that a systematic time system offset causes the observed variation (Appendix A), and conclude by advocating for further monitoring of the system (§ 5).

2. NEW TRANSITS AND SYSTEM PARAMETERS

2.1. *Observations*

WASP-4 was observed in TESS camera 2 from August 23, 2018 to September 20, during the spacecraft's second sector of science operations. The star is designated by the TESS Input Catalog as TIC 402026209 (Stassun et al. 2018).

The TESS spacecraft recorded images of WASP-4 in an 11×11 pixel array every 2 minutes. The data were downlinked via the Deep Space Network, and the Payload Operations Center then converted the timestamps from the spacecraft clock to TESS Julian Day in the *Temps Dynamique Barycentrique* (TDB) reference. The data were then processed through the Science Processing Operations Center (SPOC) pipeline at NASA Ames (Jenkins et al. 2016). SPOC used the known spacecraft trajectory to compute the barycentric time corrections on a target by target basis, and reported timestamps in "BTJD", where BTJD = BJD − 2457000, BJD is the barycentric julian date, and all times are in the TDB reference (see Urban & Seidelmann 2012 for explanations of time systems). The lightcurves were then vetted and released

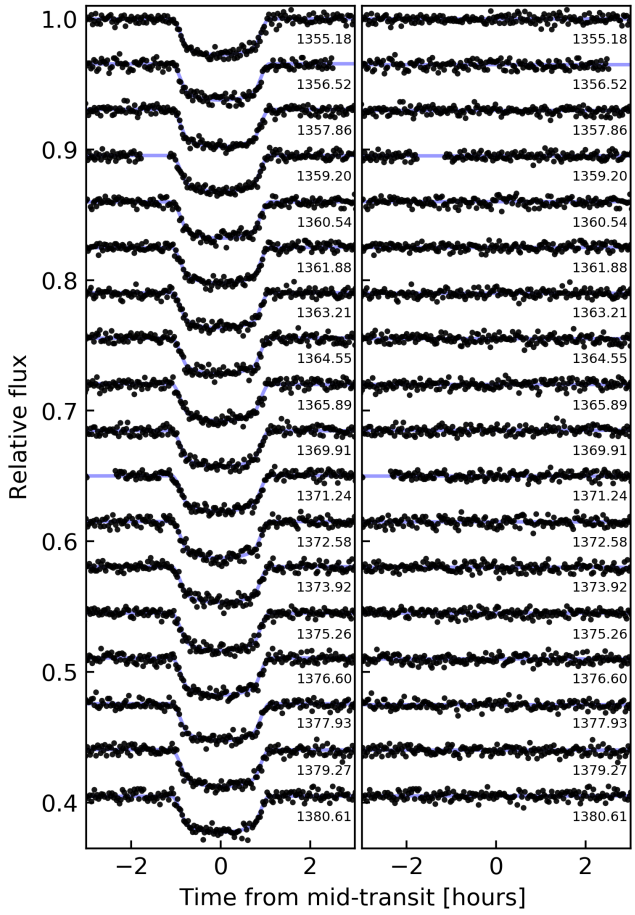

Figure 1. TESS transits of WASP-4b. On the left, black points are TESS flux measurements, with a vertical offset applied. Blue curves are best-fit models. Rounded midtimes are printed in BTJD next to the appropriate transits. The residuals are shown on the right.

by the MIT TESS Science Office to the Mikulski Archive for Space Telescopes (Ricker & Vanderspek 2018).

We began our analysis with the Presearch Data Conditioning (PDC) light curves from MAST. The steps used to find an optimal aperture (for WASP-4, a 3×3 pixel array) and the PDC-MAP algorithm are described by Smith et al. (2017a) and Smith et al. (2017b) respectively.

We processed the lightcurve as follows. First, we removed all points with non-zero quality flags. This removed data contaminated by coarse spacecraft pointing, cosmic rays, and other annoyances (Mansouri-Samani et al. 2018). We then filtered out known bad observing windows. The data closest to spacecraft perigee typically show ramp-like systematics, so we clipped out the first and last hour of both orbits. Next, we focused on the momentum dumps. As described in the data release notes[1], during the first two TESS sectors, every 2.5 days the spacecraft's reaction wheels were reset to maintain pointing stability. These events were assigned quality flags corresponding to "Reaction Wheel Desaturation Event" and "Manual Exclude". For WASP-4, these flags were simultaneously set for 54 distinct cadences, and there were 10 momentum dumps, averaging about 10 minutes of flagged data per dump. Simply out of caution, we clipped out an additional 10 minutes before and after every momentum dump. Before applying any filters, we had 19737 data points. After applying all the filters, we were left with 18165 measurements, or 92% of the original data.

After "cleaning" the data, we normalized the flux measurements by dividing out the median flux. We then converted the timestamps from BTJD to BJD by adding the appropriate 2457000 day offset (Mansouri-Samani et al. 2018). Many of these and subsequent processing steps were performed using `astrobase` (Bhatti et al. 2018) We opted not to "flatten" the lightcurves at this stage, as is often done with *e.g.*, a spline or gaussian process regression. Such procedures are asymmetric about the transit minimum and can skew the transit time measurement without being captured by the measurement uncertainties.

2.2. *Measuring the transit times*

Using the cleaned PDC lightcurve, we ran Box Least Squares (BLS) to determine the orbital period, and to estimate the transit duration and a reference epoch (Kovács et al. 2002). From these parameters, we isolated each transit to within ± 4 transit durations of its midtime. We then fit the phase-folded transit, using the analytic formulae calculated by Mandel & Agol (2002) and implemented by Kreidberg (2015). Specifically, we fit for a reference epoch, the planet to star radius ratio $R_p/R_\star$, the semi-major axis to stellar radius ratio $a/R_\star$, the inclination i, two quadratic limb-darkening coefficients $(u_{\rm linear}, u_{\rm quad})$, and the orbital period P. We set the eccentricity to zero.

Having defined the free and fixed parameters, we calculated an initial guess for the free parameters by maximizing the likelihood. We then sampled over the posterior using the algorithm proposed by Goodman & Weare (2010) and implemented by Foreman-Mackey et al. (2013). Table 1 gives the results, which are in reasonable agreement with the parameters reported by Gillon et al. (2009b), Southworth et al. (2009), and Huitson et al. (2017).

To measure mid-transit times, we then focused on each individual transit window. We fit for a model transit, plus a local linear trend. We allowed four free parameters per transit: the time of mid-transit $t_{\rm tra}$, the planet-to-star radius ratio $R_p/R_\star$, and the slope and intercept of the line. We fixed the remaining parameters – $a/R_\star$, i, P, and the limb-darkening coefficients – to the best-fit values from the global fit.

After completing an initial fit for each transit, we set the photometric error bars to be equal to the standard deviation of the out-of-transit points of the residual lightcurve. We then reperformed the fitting procedure, using the empirically determined photometric errors.

To verify that the measured uncertainties are plausible, we computed the reduced χ^2 for a linear ephemeris fit to the

[1] archive.stsci.edu/hlsps/tess-data-alerts/hlsp_tess-data-alerts_tess_phot_s01_tess_v1_release-notes.pdf

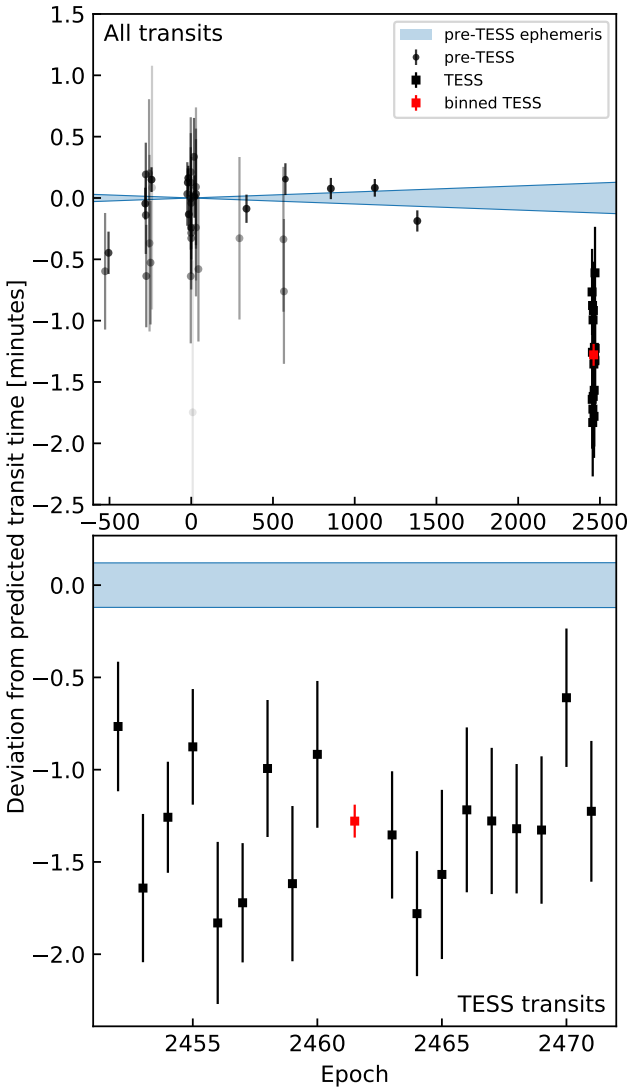

Figure 2. TESS saw WASP-4b transit earlier than expected. Both plots show observed transit times minus the pre-TESS ephemeris as a function of transit number. Blue curves are the $\pm 1\sigma$ credible interval around the constant-period prediction. *Top:* The full timing dataset spans 10 years. Less precise points are more transparent. *Bottom:* The binned TESS observation (red point) arrived 77.8 ± 10.8 seconds before it was expected.

measured TESS transit times. We found that $\chi^2 = 8.4$, with 16 degrees of freedom. Visually inspecting residuals showed that the error variance had been overestimated, so we multiplied the measured TESS errors by a factor $f = 0.73$, forcing a reduced χ^2 of unity. This lowered the mean midtime uncertainty for each transit from 30 to 22 seconds.

Figure 1 shows the light curves, best-fit models, and residuals. Table 2 reports the mid-transit times and their uncertainties. Binning the residuals to 1-hour windows and taking the median absolute deviation, the lightcurves have an RMS

Table 1. Selected system parameters of WASP-4b

Parameter	Value	Uncertainty	Comment
Transit/RV parameters:			
$R_p/R_\star$	0.1538	± 0.0013	A
i [deg]	88.52	+0.39, −0.26	A
$a/R_\star$	5.463	+0.025, −0.020	A
$u_{\rm linear}$	0.*XXX*	+0.*XXX*, −0.*XXX*	A
$u_{\rm quad}$	0.*XXX*	+0.*XXX*, −0.*XXX*	A
K [m s^{-1}]	241.1	+2.8, −3.1	B
Stellar parameters:			
$T_{\rm eff}$ [K]	5400	± 90	C
$\log g_\star$ [cgs]	4.47	± 0.11	C
[Fe/H]	−0.07	± 0.19	C
$F_{\rm bol}$ [erg cm^{-2} s^{-1}]	2.802×10^{-10}	$\pm 0.076 \times 10^{-10}$	D
π [mas]	3.7145	0.0517	F
$R_\star$ [R$_\odot$]	0.893	± 0.034	E
$\rho_\star$ [g cm^{-3}]	1.722	+0.024, −0.019	E
$M_\star$ [M$_\odot$]	0.870	+0.085, −0.077	E
T magnitude	11.778	± 0.018	G
Planetary parameters:			
a [AU]	0.0227	± 0.0007	E
M_p [M$_{\rm Jup}$]	1.192	+0.091, −0.086	E
R_p [R$_{\rm Jup}$]	1.337	± 0.048	E

NOTE— (A) From TESS lightcurves (§ 2.2). Orbital periods from timing data are in Table 4. (B) (Triaud et al. 2010). (C) From HARPS spectra (Doyle et al. 2013). (D) Stassun et al. (2017). (E) From functions of stellar, transit or RV parameters as discussed in text. (F) *Gaia* DR2. (G) Stassun et al. (2018).

of 586 ppm hr$^{1/2}$. The predicted[2] photon-counting noise is 410 ppm hr$^{1/2}$. At $T \approx 11.8$, with a 9-pixel aperture read noise is expected to contribute an additional 202 ppm hr$^{1/2}$ in quadrature. The predicted zodiacal background contribution is 673 ppm hr$^{1/2}$, based on the Winn (2013) model, which Sullivan et al. (2015) used in planet detection simulations. This zodiacal noise prediction seems to have been an overestimate, given the observed RMS of WASP-4. A more detailed assessment of TESS's photometric performance is beyond the scope of this work.

2.3. *Star and planet parameters*

Doyle et al. (2013) found accurate spectroscopic parameters for WASP-4 using high S/N HARPS spectra. Using their ($T_{\rm eff}$, $\log g$, [Fe/H]) and the available *Gaia* parallaxes, we compute the remaining system parameters empirically.

We compute the bolometric flux using broadband magnitudes from available all-sky catalogs, as follows: G from *Gaia* DR2, $B_T V_T$ from *Tycho-2*, $BVgri$ from *APASS*, JHK_S from *2MASS*, and the *WISE* 1–4 passbands, thus spanning the wavelength range 0.4–22 μm. Combining the implied angular radius with the *Gaia* DR2 parallax, and adjusting for the parallax offset (Stassun & Torres 2018), we obtain the stellar radius. For the stellar mass, we started with the $a/R_\star$ value found by Hoyer et al. (2013) from 26 ground-based transits.

[2] github.com/lgbouma/tnm

The implied semi-major axis and stellar density follow (Seager & Mallén-Ornelas 2003). Combining the density and radius gives the stellar mass. We get the planet radius using our measured $R_p/R_\star$. Finally, for the planet mass we use the observed RV semi-amplitude and inclination angle from the transit (Triaud et al. 2010; Hoyer et al. 2013).

The resulting parameters are in Table 3, and broadly agree with those of previous authors (Wilson et al. 2008; Gillon et al. 2009a; Winn et al. 2009; Southworth 2011; Petrucci et al. 2013). We use them for the remaining analysis. Comparing the empirical result to the Yonsei-Yale evolutionary track predicted by the spectroscopic parameters, we see that WASP-4 has an age ≈ 7 Gyr, and is securely in the main-sequence stage of evolution.

3. TIMING ANALYSIS

3.1. *Previous timing measurements*

Table 1 shows the transit times used in our analysis. We included data from peer-reviewed literature for which the analysis was based on observations of a single, complete transit, and for which the midpoint was fit as a free parameter. We also required that the time system be clearly documented. The occultation times are in Table 3. Since there are fewer available, we included all the occultation measurements we could find. The tabulated values have been corrected for the light-travel time across the diameter of the orbit by subtracting $2a/c = 22.8$ seconds from the observed time.

We used the homogeneous Hoyer et al. (2013) timing study as our starting point[3]. Though their latest two epochs fell slightly below the prediction of a linear ephemeris (Panel C of their Figure 6), they did not find a need to fit a quadratic function to the O-C values. We verified that all times were on the $\mathrm{BJD_{TDB}}$ time standard using the Eastman et al. (2010) calculator. We set the zero-point epoch to be as close as possible to the average of the midtimes, weighted as the inverse midtime variance. This minimizes the covariance between the transit epoch and the period (Gibson et al. 2013).

Important contributions to the timing dataset are as follows. Our earliest epoch is from EulerCam on the 1.2-m Euler telescope (Wilson et al. 2008). The second epoch comes from z-band photometry acquired by Gillon et al. (2009b) at the VLT 8.2-m with FORS2. Subsequent transits came from Winn et al. (2009)[4], Dragomir et al. (2011), Sanchis-Ojeda et al. (2011), Nikolov et al. (2012), Hoyer et al. (2013), and Ranjan et al. (2014). Finally, Huitson et al. (2017) acquired optical transmission spectra with the 8.1-m Gemini South telescope over 2011 to 2014, one transit per season. The per-point standard deviation of their lightcurves is a few hundred parts per million, within a factor of 3 from the photon noise limit. The uncertainties on their reported transit times – on average 5.6 seconds – are small, but possible given the quality of their data (Carter et al. 2008).

There are fewer available occultation times. Beerer et al. (2011) observed two occultations of WASP-4b using warm Spitzer in the 3.6 μm and 4.5 μm bands. Cáceres et al. (2011) detected an occultation from the ground in the K_s band, and gave a time in HJD, without specifying the time standard. We assumed the standard was UTC, but added $32.182 + N$ seconds of uncertainty to the reported errors, where $N = 35$ is the appropriate number of leap-seconds (see Eastman et al. 2010). Though not rigorous, this procedure inflates the error bar to a more realistic ± 94 seconds. Finally, Zhou et al. (2015) acquired occultation data from the Anglo-Australian Telescope, focusing on the eclipse depth, but also fitting for $e\cos\omega$. We converted their $e\cos\omega$ result into a midtime, using their ephemeris and the standard formula (*e.g.*, Winn 2010)

$$t_{\rm occ}(E) = t_0 + PE + \frac{P}{2}\left(1 + \frac{4}{\pi} e\cos\omega\right). \quad (1)$$

This gives us a total of 4 occultations. Although the occultation times are uncertain compared to the transits, they nonetheless help in modeling the timing variations.

3.2. *Analysis*

After collecting the literature times and measuring the TESS times, we compared the observed time to the prediction based solely on the literature times. The result is shown in Figure 2. The TESS observations arrived early. One immediate concern was systematic errors in either the archival or the TESS timestamps. The tests we used to mitigate the latter possibility are described in Appendix A.

Assuming that the observed timing variation is astrophysical, we proceeded by exploring three models for the timing data, identical to the study by Patra et al. (2017).

The first model assumes a constant orbital period on a circular orbit:

$$t_{\rm tra}(E) = t_0 + PE, \quad (2)$$

$$t_{\rm occ}(E) = t_0 + \frac{P}{2} + PE, \quad (3)$$

for E the epoch number. The two free parameters are the reference epoch t_0 and the period P.

The second model assumes a constant period derivative, and a circular orbit:

$$t_{\rm tra}(E) = t_0 + PE + \frac{1}{2}\frac{{\rm d}P}{{\rm d}E}E^2, \quad (4)$$

$$t_{\rm occ}(E) = t_0 + \frac{P}{2} + PE + \frac{1}{2}\frac{{\rm d}P}{{\rm d}E}E^2. \quad (5)$$

The three free parameters are the epoch, period at the reference epoch, and period derivative, ${\rm d}P/{\rm d}t = (1/P){\rm d}P/{\rm d}E$.

The third model assumes the planet has a slightly eccentric orbit, and that the line of apsides is rotating:

$$t_{\rm tra}(E) = t_0 + P_s E - \frac{eP_a}{\pi}\cos\omega, \quad (6)$$

$$t_{\rm occ}(E) = t_0 + \frac{P_a}{2} + P_s E + \frac{eP_a}{\pi}\cos\omega, \quad (7)$$

[3] We also tried using times directly from the original authors; the results did not change, so we opted for the Hoyer et al. (2013) times as the more homogeneous option.

[4] Winn et al. (2009) recorded the GPS clock time in UT reference. They then converted this to BJD in the TDB reference for their reported midtimes.

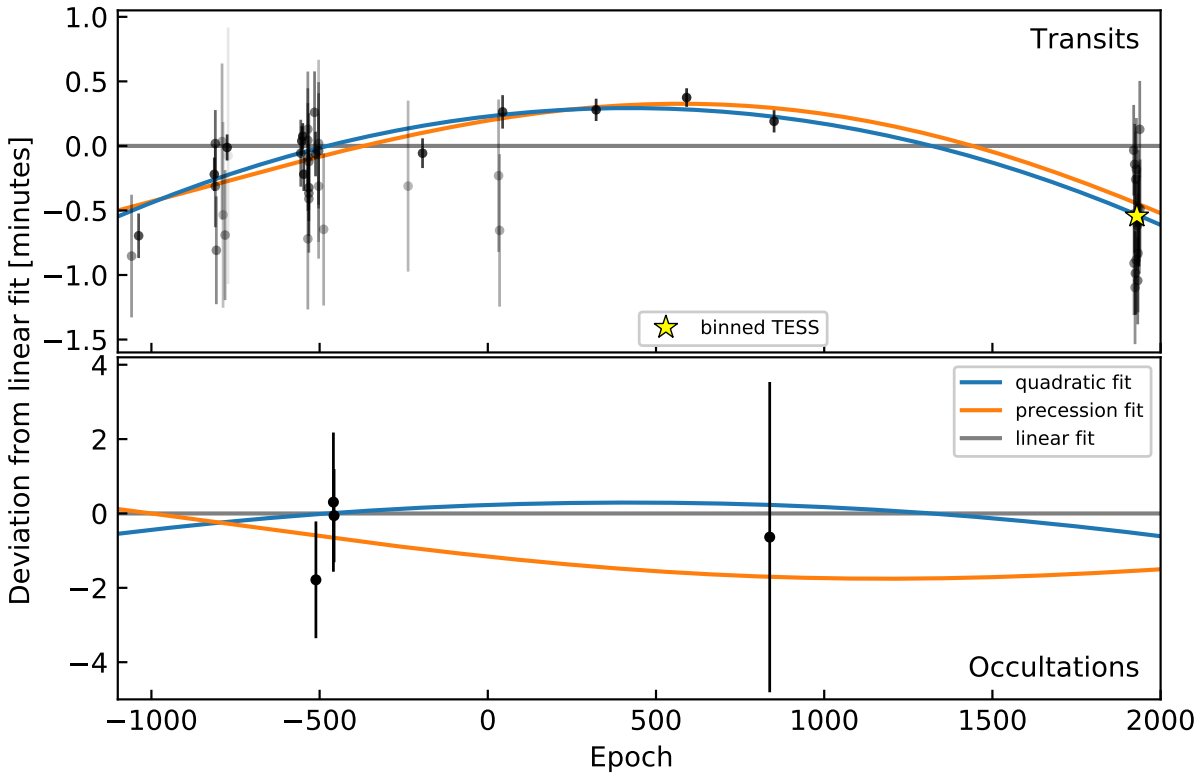

Figure 3. Timing residuals and best-fit models for WASP-4b. Points are observed transit times minus a linear fit to all observed times. Less precise times are more transparent. The best constant period model (gray line) is a poor fit to the observations. The best-fit tidal decay model (blue) and apsidal precession model (orange) can fit the data. The binned TESS point (star) is for display purposes only.

for P_s the sidereal period, e the eccentricity, P_a the anomalistic period, and ω the argument of pericenter. Following Giménez & Bastero (1995) and Patra et al. (2017), in this model the angular velocity of the line of apsides $d\omega/dE$ is constant,

$$\omega(E) = \omega_0 + \frac{d\omega}{dE}E, \tag{8}$$

and the sidereal and anomalistic periods are related by

$$P_s = P_a\left(1 - \frac{1}{2\pi}\frac{d\omega}{dE}\right). \tag{9}$$

The five free parameters are the epoch, sidereal period, eccentricity, argument of pericenter at the reference epoch, and angular velocity of line of apsides: $(t_0, P_s, e, \omega_0, d\omega/dE)$.

Figure 3 shows the residuals with respect to the linear model. The best linear fit has $\chi^2 = 149$ and 58 degrees of freedom. The best quadratic fit has $\chi^2 = 48.0$ and 57 degrees of freedom, compared to $\chi^2 = 51.0$ and 55 degrees of freedom for the best-fit precession model.

The difference in χ^2 between the linear and quadratic fit corresponds to $p \approx 10^{-23}$. Clearly, it is more likely that some systematic error could be affecting one of the most important sets of times: either the earliest times, the Huitson et al. Gemini times (epoch numbers 44, 322, 591, and 851), or the TESS times. We have taken every precaution against systematic offsets in the TESS dataset (Appendix A). Huitson et al. stand by their reported times (J.-M. Désert, priv. comm.)[5]. Since the linear model provides a poor fit to the data, we discard it from further consideration.

The quadratic model fits better than the precession model. It is favored by $\Delta\chi^2 = 3.0$, and has two fewer free parameters. Another useful heuristic for model comparison is the Bayesian Information Criterion (BIC),

$$\mathrm{BIC} = \chi^2 + k\log n, \tag{10}$$

for k the number of free parameters, and n the number of data points. For us, $n = 60$. The difference in the BIC for the precession and decay models is $\Delta\mathrm{BIC} = \mathrm{BIC}_{\mathrm{prec}} - \mathrm{BIC}_{\mathrm{quad}} = 11$, corrsonding to a Bayes factor of $\approx 4 \times 10^4$. The Akaike Information Criterion similarly favors the orbital decay model, by $\Delta\mathrm{AIC} = 7$. This is strong evidence that the quadratic model describes the data better than the precession model (Kass & Raftery 1995).

If we assume the orbital decay model, we find a period derivative

$$\dot{P} = -(3.82 \pm 0.38) \times 10^{-10} = -(12.1) \pm 0.12\,\mathrm{ms\,yr^{-1}}. \tag{11}$$

[5] Huitson et al. 2017 corrected the times to be at mid-exposure. They also analyzed other hot Jupiters, which all showed mid-transit times as expected from a constant ephemeris.

For comparison, the period derivative seen by Maciejewski et al. (2016) and Patra et al. (2017) in WASP-12b is $\dot{P} = -29 \pm 3\,\mathrm{ms\,yr^{-1}}$. If both planets are decaying, WASP-4b would be inspiraling at about half the rate as WASP-12b.

If we instead assume the precession model, the best-fit eccentricity is

$$e = (1.63^{+1.48}_{-0.65}) \times 10^{-3} \tag{12}$$

The longitude of periapse correspondingly advances by $\dot{\omega} = 14.8^{+5.4}_{-3.8}$ degrees yr^{-1}, and the precession period would be 24^{+8}_{-6} years.

The median parameters and their standard deviations are reported for the three models in Table 4. In short, a linear ephemeris does not describe the observed times. Both orbital decay and precession can fit the data, but the precession model is statistically disfavored.

4. IMPLICATIONS

4.1. *Orbital decay*

The middle panel of Figure 4 shows the expected orbital decay time of WASP-4b compared to other transiting giant planets. Though roughly 20 hot Jupiters have shorter predicted decay times, most are not as well-observed as WASP-4b. Moreover, some hot Jupiters, *e.g.*, WASP-18b, orbit fully radiative stars, which may dissipate tidal energy less efficiently than stars that are partially convective.

For the sake of argument, let us assume that the timing variation is caused entirely by orbital decay. If the period decreases at a fixed rate, then it will reach zero after

$$\frac{P}{\dot{P}} = 9.6\,\mathrm{Myr}. \tag{13}$$

For comparison, the survival time found by Patra et al. (2017) for WASP-12b was 3.2 Myr.

Let us assume further that the "constant phase lag" model for tidal interaction in a binary applies (Zahn 1977). The fluid response is parametrized by a modified[6] quality factor, $Q'_\star = 3Q_\star/(2k_\star)$. Here $k_\star$ is the stellar Love number, which is smaller when the star's density distribution is more centrally concentrated. $Q_\star$ is the ratio of the energy stored in the equilibrium deformation of the star, divided by the energy lost to heat per tidal period (*e.g.*, Goldreich & Soter 1966). A larger $Q_\star$ implies less efficient tidal dissipiation. Though the fluid mechanics responsible for the dissipation should depend on the amplitude and frequency of the tidal perturbation (Ogilvie 2014, Section 3.3), we will treat $Q'_\star$ as a constant. This should not be taken literally; $Q'_\star$ may in fact change sharply as the tidal frequency changes (Penev et al. 2018).

If the planet's spin and orbit are synchronized, the star is slowly rotating, and the eccentricity is small, then the semi-major axis and eccentricity evolve as (Appendix B of Met-

[6] For stars, $k_\star \sim \mathcal{O}(10^{-2})$, so it is important to explicitly distinguish $Q'_\star$ from $Q_\star$ (*e.g.*, Schwarzschild 1958).

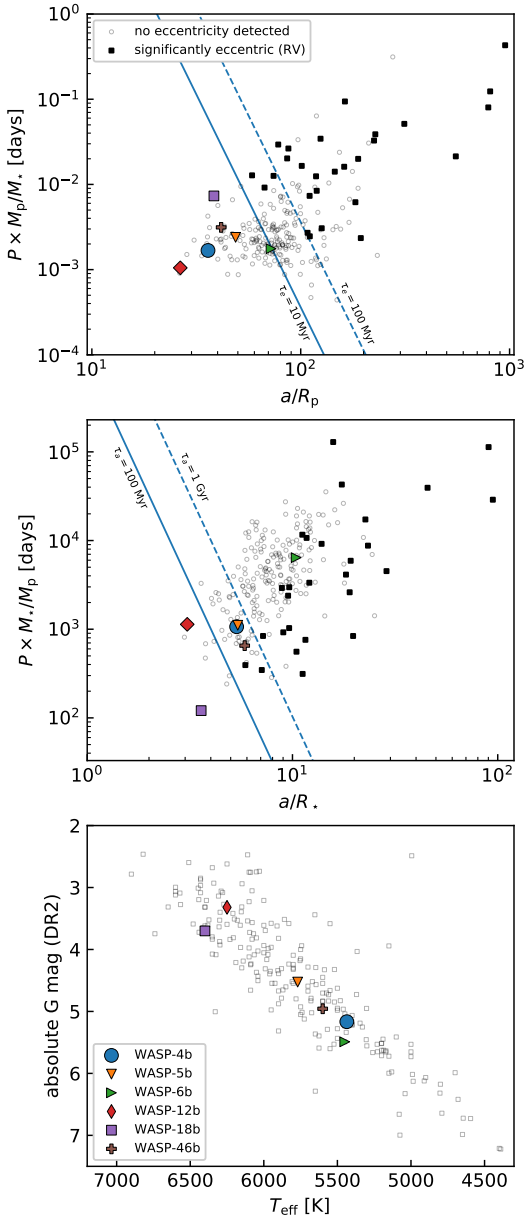

Figure 4. WASP-4b has a short eccentricity damping time and a medium decay time compared to other hot Jupiters. It seems to orbit a main sequence host. *Top:* Points are transiting giant planets from Bonomo et al. (2017), who measured the eccentricities using radial velocities. Solid squares (including WASP-18b) have significant eccentricity detections. The axes are chosen so that constant eccentricity damping timescales (Equation 14) are lines. The contours shown assume $Q'_p = 10^5$. *Middle:* Axes are chosen so to that constant orbital decay timescales (Equation 15) are lines. The contours shown assume $Q'_\star = 10^7$. *Bottom:* HR diagram highlighting WASP-12b, which shows timing variations similar to WASP-4b. We also show hot Jupiters for which we detect no timing variation (see § A.2).

zger et al. 2012)

$$\frac{1}{\tau_e} = \frac{|\dot{e}|}{e} = \frac{63\pi}{2Q'_p}\left(\frac{R_p}{a}\right)^5\left(\frac{M_\star}{M_p}\right)\left(\frac{1}{P}\right) \quad (14)$$

$$\frac{1}{\tau_a} = \frac{|\dot{a}|}{a} = \frac{9\pi}{Q'_\star}\left(\frac{R_\star}{a}\right)^5\left(\frac{M_p}{M_\star}\right)\left(\frac{1}{P}\right). \quad (15)$$

The orbital period evolves as

$$\dot{P} = -\frac{27\pi}{2Q'_\star}\left(\frac{M_p}{M_\star}\right)\left(\frac{R_\star}{a}\right)^5. \quad (16)$$

The modified quality factor of WASP-4 corresponding to the observed value of $\dot{P}$ would then be

$$Q'_\star \approx 3.3 \times 10^4. \quad (17)$$

This is rather small. Jupiter has $Q'_{\rm Jup} \approx 1.4 \times 10^5$, based on the orbits of the Galilean moons (Lainey et al. 2009). For stars, studies of the binary eccentricity distribution have yielded $Q'_\star \approx 10^5 - 10^7$ (*e.g.*, Meibom & Mathieu 2005; Belczynski et al. 2008; Geller et al. 2013; Milliman et al. 2014). The dissipation rates may differ in hot Jupiter systems, since the tidal forcing frequencies and amplitudes are different. Observationally-driven studies of hot Jupiter systems have found $Q'_\star \approx 10^5 - 10^8$, from quite different models (Jackson et al. 2009; Hansen 2010; Penev et al. 2012, 2018; Collier Cameron & Jardine 2018). For instance, motivated by the rapid rotation of some hot Jupiter hosts (Pont 2009; Penev et al. 2016), Penev et al. (2018) modeled the evolution of hot Jupiter systems under the influence of a magnetized wind and a constant phase-lag tide. For WASP-4, their method gave $Q'_\star \approx (1.2^{+1.0}_{-0.5}) \times 10^7$. This disagrees strongly with the value we infer from the apparent period change.

Essick & Weinberg (2016) proposed a theoretically-motivated tidal dissipation model , in which a coupled network of gravity modes would be excited at the base of the stellar convective zone, and would brake near the stellar core to provide the needed dissipation. In their approach, the stellar quality factors in hot Jupiter systems vary from $Q'_\star \approx 10^5 - 10^6$. From their Equation 26, the predicted quality factor for WASP-4 is $Q'_\star = 7 \times 10^5$. This is an order of magnitude larger than implied by the observed period change.

The applicability of the Essick & Weinberg (2016) model depends on the evolutionary state of the star. The bottom panel of Figure 4 shows WASP-4 in the context of giant planet hosts from the Bonomo et al. (2017) sample. On the y-axis is $G = g - \mu$, for g the apparent Gaia-band magnitude, and μ the distance modulus reported by Gaia Collaboration et al. (2018). The x-axis is the effective temperature from Bonomo et al. (2017), which for WASP-4 agrees within 1σ of that from Table 2. Inspecting the HR diagram, WASP-4 shows litle evidence of being evolved, in agreement with our analysis from § 2.3.

In summary, if the observed period change is caused entirely by tidal decay, it would imply a tidal dissipation efficiency stronger than most predictions. It might be possible that we are observing at a special time, shortly after the planet's inward migration, or when the planet is near resonance with a stellar oscillation mode. Tidal dissipation rates might also be increased if the star is turning off the main sequence. A final possibility is that an exterior planet could be trapping WASP-4b's spin vector in a high-obliquity state, causing planetary obliquity tides as suggested for WASP-12b (Millholland & Laughlin 2018). For now, all of these explanations seem strained; it is unclear that tidal decay can explain the observed timing variations by any mechanism that we have considered.

4.2. *Apsidal precession*

Let us instead assume that the timing variation can be explained as being a portion of an apsidal precession cycle. The required orbital eccentricity is then $e \approx 1.6 \times 10^{-3}$, and one full precession period would take about 24 years.

Ragozzine & Wolf (2009) calculated apsidal precession periods for hot Jupiters ranging between of order 10 and 100 years. They highlighted that for many hot Jupiters, including WASP-4b, over 90% of the apsidal precession comes from the tidal bulge of the planet. Precession from general relativity, the planet's rotational bulge, and the star's rotational and tidal bulges are minor additions.

Ragozzine & Wolf (2009) also noted that if the planet has non-zero eccentricity, a measurement of $\dot{\omega}$ can be used to measure the planet's Love number, $k_{2,p}$. From their Equation 14, the implied Love number for WASP-4b is

$$k_{2,p} = 1.6^{+2.1}_{-1.2}. \quad (18)$$

For comparison, $k_{2,\rm Jup} \approx 0.55$ (Wahl et al. 2016; Ni 2018). A uniform density sphere has $k_2 = 1.5$. The uncertainties on $k_{2,p}$ are large because the eccentricity, reference time, and $d\omega/dE$ are correlated, and the measured occultation times only barely constrain them (Figure 5).

4.2.1. *Observations of small eccentricities in hot Jupiter systems*

Could the eccentricity truly be non-zero? For WASP-4b, the eccentricity damping timescale (Equation 14) is $\tau_e = 0.29(Q'_p/10^5)$ Myr. The system is well over 1 Gyr (Winn et al. 2009) old, so any initial eccentricity should have been erased.

The top panel of Figure 4 compares the expected eccentricity damping time of WASP-4b with other transiting giant planets. WASP-4b has one of the shortest known eccentricity damping times. The hot Jupiter with the nearest τ_e and a significant measured eccentricity is WASP-18b, with $e = 0.0076 \pm 0.0010$ (Triaud et al. 2010; Bonomo et al. 2017). This is the smallest significant eccentricity measured by the RV method, with the next-smallest cases being HAT-P-20b ($e = 0.01580^{+0.0023}_{-0.0018}$), and WASP-38b ($e = 0.02780^{+0.003}_{-0.0028}$).

Occultation timing can provide stronger eccentricity limits than RV measurements, but they often come with caveats. For WASP-4b, the strongest limit on its eccentricity comes from Beerer et al. (2011), who observed occultations and derived a 2σ upper limit on $|e\cos\omega|$ of 0.0024. Placing eccentricity limits stronger than $e < 10^{-3}$ has only been possible for a few hot Jupiters, and with numerous false-starts. HD

189733b, for example, was initially reported to have a non-zero eccentricty (Knutson et al. 2007). This result was retracted by Agol et al. (2010), who used a larger dataset of 7 Spitzer occultations and found a smaller average offset in the occultation time than Knutson et al. (2007). Agol et al. (2010) also noted that a larger fraction of the planet's observed occultation time offset could be explained by detailed modeling of the planetary hot-spot, which can shift occultation times by up to a few minutes (Williams et al. 2006). Including an updated hot-spot model, Agol et al. (2010) reported $e\cos\omega < 0.00023$ at 2σ, perhaps the strongest eccentricity limit in place for a hot Jupiter. Similar sagas transpired for HD 209458b and WASP-12b, with early reports of small non-zero eccentricities (Winn et al. 2005; Hebb et al. 2009; López-Morales et al. 2010), only to be ruled out by the limits of subsequent followup: $|e\cos\omega| < 0.0007$ for HD 209458b, and $|e\cos\omega| < 0.0040$ (2σ) for WASP-12b (Crossfield et al. 2012; Campo et al. 2011; Croll et al. 2011).

To summarize, empirical constraints on the ellipticity of hot Jupiter orbits at the $e \lesssim 10^{-3}$ level are present only for HD 189733b and HD 209458b, from occultation timing. Once the timing offsets are of order tens of seconds, eccentricities from occultation timing may have systematic uncertainties because of the hot-spot issue (Williams et al. 2006; Agol et al. 2010). Except for WASP-18b, radial velocity measurements have provided eccentricity constraints only at the $e > 10^{-2}$ level. We therefore cannot empirically rule out hot Jupiter eccentricities at the level needed to assess WASP-4's putative eccentricity.

4.2.2. *Theoretical expectations for small eccentricities in hot Jupiter systems*

Lacking empirical data, we turn to theoretical mechanisms that could produce small eccentricities.

Neighboring companion—Mardling (2007) considered the long-term tidal evolution of hot Jupiters with companions. They pointed out that although the early phases of the two-planet eccentricity evolution occur quickly, the final phase of the joint eccentricity evolution towards circularity would occur on timescales several orders of magnitude longer than the circularization time (see their Figures 4 and 5). The companion in their model is coplanar, and can have a mass down to an Earth-mass; the main requirement is that both the hot Jupiter and the outer companion start on eccentric orbits.

Another way to excite the hot Jupiter's eccentricity is the Kozai-Lidov mechanism (Lidov 1962; Kozai 1962). In this case, the orbital plane of the outer companion, "c", would need to be inclined relative to that of the hot Jupiter, "b", by at least $\sin^{-1}\sqrt{2/5} \approx 39°$. For the Kozai-Lidov mechanism to operate at maximum efficiency, from Bailey & Goodman (2019) Equation 20 we need

$$M_c > 7.7\,M_\oplus \times \left(\frac{a_c}{a_b}\right)^{3/2}, \tag{19}$$

where $M_{b,c}$ and $a_{b,c}$ are the mass and semi-major axis of WASP-4b and the hypothetical WASP-4c, and we have assumed WASP-4b's Love number is $k_{2,b} \approx 0.6$. For the RV signal of the companion to remain undetected, it would need to be in the residual $(O-C)_{RV} = 15.2\,ms^{-1}$ reported by Triaud et al. (2010). Again following Bailey & Goodman (2019), this implies

$$M_c < (O-C)_{RV}\left(\frac{M_\star a_b}{G}\right)^{1/2}\left(\frac{a_c}{a_b}\right)^{1/2} f^{-1/2}$$
$$M_c < 24.2\,M_\oplus \times \left(\frac{a_c}{a_b}\right)^{1/2} f^{-1/2}, \tag{20}$$

for $f(e_c,\omega_c,i_c) \propto \sin^2 i_c$ a geometric prefactor that depends on the argument of periastron ω_c and inclination i_c of the exterior companion (Bailey & Goodman 2019 Equation 23). Since WASP-4b transits along the line of sight, f can be arbitrarily small, and both of the preceding limits can be satisfied.

While either of the two preceding mechanisms could produce the needed eccentricity, it would be more satifying if long-term radial velocity monitoring showed an additional planet in the system. The chances of one existing with a mass between 1-13 M_{Jup} and orbital semi-major axis between 1-20 AU is about 50%, and a linear trend is currently present at $\sim 2\sigma$ (Knutson et al. 2014).

Fluctuations in the gravitational potential from convection—A separate mechanism to pump the eccentricity involves the gravitational fluctuations from stellar convection (Phinney 1992, Section 7). Phinney presents this idea by analogy with a pendulum, which is never really at rest. Instead, collisions with air molecules randomly perturb its momentum and energy, and the equipartition theorem of statistical mechanics tells us the average energy is $\langle E_{pend}\rangle = kT_{air}$. In hot Jupiter systems, the "air molecules" are convective eddies, and their associated kinetic energy perturbs the orbit away from circularity. In particular, from Phinney 1992 Equation 7.33,

$$\langle e^2\rangle = \frac{2\langle E_e\rangle}{\mu n^2 a^2} = 6.8\times10^{-5}\frac{(L^2R_{conv}^2M_{conv}^2)^{1/3}}{\mu n^2 a^2}, \tag{21}$$

for L the stellar luminosity, R_{conv} (M_{conv}) the width (mass) of the convective region, μ the reduced mass, n the orbital frequency, and a the semi-major axis. For WASP-4, convection in the star is more important than convection in the planet, and $\langle e^2\rangle^{1/2} \lesssim 10^{-5}$.

4.3. *Applegate effect*

Some eclipsing binaries exhibit period modulations with amplitudes of $\lesssim 0.05$ days over timescales of decades (*e.g.*, Söderhjelm 1980; Hall 1989). Applegate (1992) proposed a mechanism to explain these modulations in which the internal structure of a magnetically active star changes shape via cyclic exchange of angular momentum between the inner and outer zones of the star. This model could also apply to a hot Jupiter orbiting a star with a convective zone. The changing gravitational quadrupole of the star would cause the orbit of the planet to precess on the timescale of the stellar activity

cycle ("the dynamo timescale"). An essential difference between this process and apsidal precession is that it is expected to be quasi-periodic (*e.g.*, Söderhjelm 1980, Figure 12). The transit and occultation deviations would also have the same sign, while for apsidal precession they have opposite signs. For WASP-4, Watson & Marsh (2010) estimated that the effect could produce timing deviations of up to 15 seconds, depending on the modulation period of the stellar dynamo, and the corresponding level of differential surface shear. This cannot explain the majority our observed 78 second variation.

4.4. *Other possible explanations*

Another mechanism to produce the observed period change would be if an unseen companion in the WASP-4 system accelerated the star towards us. This would produce a period derivative

$$\dot{P} \approx \frac{\dot{v}_r P}{c}, \tag{22}$$

for $\dot{v}_r$ the time derivative of the radial velocity. Knutson et al. (2014) collected 5 Keck HIRES radial velocity measurements for WASP-4, and merged them with measurements from CORALIE and HARPS (Wilson et al. 2008; Pont et al. 2011; Husnoo et al. 2012). Using these datasets, Knutson et al. (2014) found

$$\dot{v}_r = -0.0099^{+0.0052}_{-0.0054}\,\mathrm{m\,s^{-1}\,day^{-1}}, \tag{23}$$

or that the star can be accelerating towards us at most by $\dot{v}_r > -0.021\,\mathrm{m\,s^{-1}\,day^{-1}}$ (2σ). The associated $\dot{P}$ must be less than 9×10^{-11}. Radial acceleration could thus cause at most one-quarter of the observed period decrease (Equation 11). Improved radial velocity monitoring will help clarify the situation, particularly given the fact that WASP-4 shows short-term trends with amplitudes 100 times larger, over tens of days (Husnoo et al. 2012). Given the known activity of the system (Sanchis-Ojeda et al. 2011), these short-timescale variations might conspire to produce spurious measurements over long baselines.

There are two other small effects worth noting. The first is the Shklovskii (1970) effect, in which the star's proper motion leads to a changing radial velocity. This would be apparent in the Doppler measurements described above. The effect contributes a change of order $\dot{P} \sim P\mu^2 d/c \sim 6 \times 10^{-13}$. The second effect, described by Rafikov (2009), comes from the star's on-sky motion altering our viewing angle, and leads to an observed apsidal precession. The corresponding period change is $\dot{P} \sim (P\mu)^2/2\pi \sim 10^{-21}$.

Many of the phenomena discussed could presumably occur simultaneously. We found though that radial acceleration, proper-motion, and the Applegate mechanism are unlikely to explain the majority of the timing deviations. Tidal decay seems implausible, given the high level of dissipation required. This leaves apsidal precession as the most plausible explanation, but more data are needed for a definitive interpretation.

5. FUTURE PROSPECTS

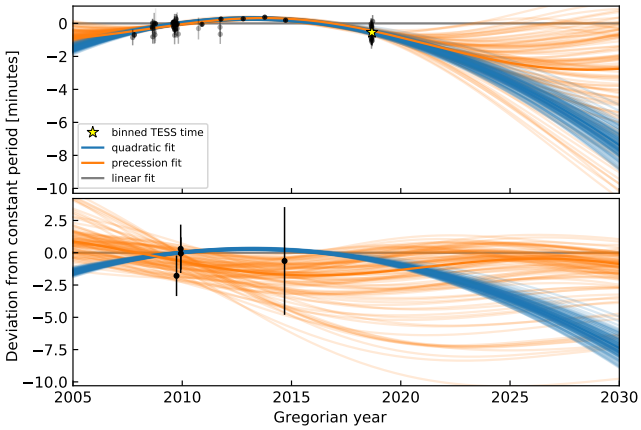

Figure 5. Further observations will be needed to confirm and understand the timing variations of WASP-4b. Dots are as in Figure 3. Lines are 100 random draws from the posteriors of the apsidal precession model (orange), and the orbital decay model (blue).

If TESS continues observing after its primary mission, it will observe additional transits of WASP-4b in the early 2020s (Figure 5). High-precision ground-based transit measurements could also be useful. In order to rule between orbital decay and apsidal precession, occultation measurements in both the near term and also in the mid-2020s will be needed. Additionally, confirmation and extension of the linear RV trend suggested by Knutson et al. (2014) would help in understanding whether an exterior companion in the system might explain any residual eccentricity. These observations should be carried out because they will lead to new knowledge; either a measure of the stellar tidal dissipation efficiency, or the eccentricity and Love number of the planet. Either outcome for a single system would be somewhat interesting. In the coming decade, wide-field photometric surveys (TESS, HATPI, NGTS, PLATO) might even enable such measurements at a population level, which would be extremely interesting.

L.G.B. gladly acknowledges helpful discussions with A. Bailey, F. Dai and V. Van Eylen, and is grateful to the people who have turned TESS from an idea into reality. WASP-4 was included on the "short-cadence" target list thanks to the Guest Investigator programs of J. Southworth and S. Kane (G011112 and G011183 respectively). This paper includes data collected by the TESS mission, which are publicly available from the Mikulski Archive for Space Telescopes (MAST). Funding for the TESS mission is provided by NASA's Science Mission directorate. This research has made use of the NASA Exoplanet Archive, which is operated by the California Institute of Technology, under contract with the National Aeronautics and Space Administration under the Exoplanet Exploration Program. This work made use of NASA's Astrophysics Data System Bibliographic Services. This research has made use of the VizieR catalogue access tool, CDS, Strasbourg, France.

The original description of the VizieR service was published in A&AS 143, 23. This work has made use of data from the European Space Agency (ESA) mission *Gaia* (https://www.cosmos.esa.int/gaia), processed by the *Gaia* Data Processing and Analysis Consortium (DPAC, https://www.cosmos.esa.int/web/gaia/dpac/consortium). Funding for the DPAC has been provided by national institutions, in particular the institutions participating in the *Gaia* Multilateral Agreement.

Facility: TESS (Ricker et al. 2015), Gaia (Gaia Collaboration et al. 2016, 2018)

Software: `astrobase` (Bhatti et al. 2018), `astropy` (Collaboration et al. 2018), `astroquery` (Ginsburg et al. 2018), `BATMAN` (Kreidberg 2015), `corner` (Foreman-Mackey 2016), `emcee` (Foreman-Mackey et al. 2013), `IPython` (Pérez & Granger 2007), `matplotlib` (Hunter 2007), `numpy` (Walt et al. 2011), `pandas` (McKinney 2010), `scikit-learn` (Pedregosa et al. 2011), `scipy` (Jones et al. 2001).

Table 2. WASP-4b transit times, uncertainties, and references.

t_{tra} [BJD_{TDB}]	$\sigma_{t_{tra}}$ [days]	Epoch	H13?	Reference
2454368.59279	0.00033	-1059	1	Wilson et al. (2008)
2454396.69576	0.00012	-1038	1	Gillon et al. (2009b)
2454697.79817	0.00009	-813	1	Winn et al. (2009)
2454701.81280	0.00022	-810	1	Hoyer et al. (2013)
2454701.81303	0.00018	-810	1	Hoyer et al. (2013)
2454705.82715	0.00029	-807	1	Hoyer et al. (2013)
2454728.57767	0.00042	-790	1	Hoyer et al. (2013)
2454732.59197	0.00050	-787	1	Hoyer et al. (2013)
2454740.62125	0.00035	-781	1	Hoyer et al. (2013)
2454748.65111	0.00007	-775	1	Winn et al. (2009)
2454752.66576	0.00069	-772	1	Dragomir et al. (2011)
2455041.72377	0.00018	-556	1	Hoyer et al. (2013)
2455045.73853	0.00008	-553	1	Sanchis-Ojeda et al. (2011)
2455049.75325	0.00007	-550	1	Sanchis-Ojeda et al. (2011)
2455053.76774	0.00009	-547	1	Sanchis-Ojeda et al. (2011)
2455069.82661	0.00029	-535	1	Nikolov et al. (2012)
2455069.82670	0.00028	-535	1	Nikolov et al. (2012)
2455069.82617	0.00038	-535	1	Nikolov et al. (2012)
2455069.82676	0.00031	-535	1	Nikolov et al. (2012)
2455073.84128	0.00026	-532	1	Nikolov et al. (2012)
2455073.84108	0.00029	-532	1	Nikolov et al. (2012)
2455073.84111	0.00023	-532	1	Nikolov et al. (2012)
2455073.84114	0.00018	-532	1	Nikolov et al. (2012)
2455096.59148	0.00022	-515	1	Hoyer et al. (2013)
2455100.60595	0.00012	-512	1	Sanchis-Ojeda et al. (2011)
2455112.64986	0.00039	-503	1	Nikolov et al. (2012)
2455112.65009	0.00033	-503	1	Nikolov et al. (2012)
2455112.65005	0.00031	-503	1	Nikolov et al. (2012)
2455112.65005	0.00049	-503	1	Nikolov et al. (2012)
2455132.72310	0.00041	-488	1	Hoyer et al. (2013)
2455468.61943	0.00046	-237	1	Hoyer et al. (2013)
2455526.16356	0.00008	-194	0	Ranjan et al. (2014)
2455828.60375	0.00041	32	1	Hoyer et al. (2013)
2455832.61815	0.00041	35	1	Hoyer et al. (2013)
2455844.66287	0.00009	44	0	Huitson et al. (2017)
2456216.69123	0.00006	322	0	Huitson et al. (2017)
2456576.67556	0.00005	591	0	Huitson et al. (2017)
2456924.61561	0.00006	851	0	Huitson et al. (2017)
2458355.18490	0.00024	1920	0	This work
2458356.52251	0.00026	1921	0	This work
2458357.86101	0.00024	1922	0	This work
2458359.19951	0.00025	1923	0	This work
2458360.53708	0.00027	1924	0	This work
2458361.87539	0.00024	1925	0	This work
2458363.21412	0.00027	1926	0	This work
2458364.55192	0.00025	1927	0	This work
2458365.89064	0.00026	1928	0	This work
2458369.90503	0.00027	1931	0	This work
2458371.24297	0.00026	1932	0	This work
2458372.58136	0.00027	1933	0	This work
2458373.91982	0.00027	1934	0	This work
2458375.25801	0.00024	1935	0	This work
2458376.59621	0.00024	1936	0	This work
2458377.93443	0.00026	1937	0	This work
2458379.27317	0.00026	1938	0	This work
2458380.61097	0.00027	1939	0	This work

Table 2 continued

Table 2 *(continued)*

NOTE— t_{tra} is the measured transit midtime, and $\sigma_{t_{tra}}$ is its 1σ uncertainty. σ_{t_0} was evaluated from the sampled posteriors by taking the maximum of the difference between the 84th percentile minus the median, and the median minus the 16th percentile. The "Reference" column refers to the work describing the original observations. The "H13?" column is 1 if the mid-time value was taken from Hoyer et al. (2013). Otherwise, the mid-time came from the column listed in "Reference". The Hoyer et al. (2013) BJD_{TT} times are equal to BJD_{TDB} for our purposes (Urban & Seidelmann 2012). We omitted the timing measurements from Southworth et al. (2009), since there were technical problems with the computer clock at the time of observation (Nikolov et al. 2012).

Table 3. WASP-4b occultation times, uncertainties, and references.

t_{occ} [BJD_{TDB}]	$\sigma_{t_{occ}}$ [days]	Epoch	Reference
2455102.61210	0.00109	-511	Cáceres et al. (2011)[a]
2455172.20159	0.00130	-459	Beerer et al. (2011)
2455174.87780	0.00087	-457	Beerer et al. (2011)
2456907.88714	0.00290	838	Zhou et al. (2015)[b]

NOTE— t_{occ} is the measured occultation midtime, minus the $2a/c$ = 22.8 second light travel time; $\sigma_{t_{occ}}$ is the 1σ uncertainty on the occultation time.

[a] Cáceres et al. (2011) reported this time in "HJD", with an unspecified time standard. We assumed the time was originally in HJD_{UTC}, inflated the uncertainties by 67.184 seconds, and converted to BJD_{TDB} for the time reported.

[b] Zhou et al. (2015) fixed the epoch, and let $e\cos\omega$ float. Using the reported dates of observation, we converted their $e\cos\omega$ values into an occultation time using Equation 1 of the text.

Table 4. Best-fit model parameters.

Parameter	Median Value (Unc.)[a]
Constant period	
t_0 [BJD_{TBD}]	2455785.780502(+19)(-19)
P [days]	1.338231460(+22)(-22)
Constant period derivative	
t_0 [BJD_{TBD}]	2455785.780664(+24)(-25)
P [days]	1.338231677(31)(-31)
dP/dt	$-3.83(+39)(-36) \times 10^{-10}$
Apsidal precession	
t_0 [BJD_{TBD}]	2455785.78015(+22)(-29)
P_s [days]	1.33823131(+16)(-34)
e	$1.59^{+1.38}_{-0.64} \times 10^{-3}$
ω_0 [rad]	2.37(+35)(-30)
$d\omega/dE$ [rad epoch^{-1}]	$9.56^{+3.55}_{-2.43} \times 10^{-4}$

[a] The numbers in parenthesis give the 1σ uncertainty in the final two digits, where appropriate.

REFERENCES

Agol, E., Cowan, N. B., Knutson, H. A., et al. 2010, The Astrophysical Journal, 721, 1861

Anderson, D. R., Gillon, M., Hellier, C., et al. 2008, Monthly Notices of the Royal Astronomical Society, 387, L4

Anderson, D. R., Collier Cameron, A., Gillon, M., et al. 2012, Monthly Notices of the Royal Astronomical Society, 422, 1988

Applegate, J. H. 1992, The Astrophysical Journal, 385, 621

Bailey, A., & Goodman, J. 2019, Monthly Notices of the Royal Astronomical Society, 482, 1872

Barnes, J. W., van Eyken, J. C., Jackson, B. K., Ciardi, D. R., & Fortney, J. J. 2013, The Astrophysical Journal, 774, 53

Batygin, K., Bodenheimer, P., & Laughlin, G. 2009, The Astrophysical Journal, 704, L49

Beerer, I. M., Knutson, H. A., Burrows, A., et al. 2011, The Astrophysical Journal, 727, 23

Belczynski, K., Kalogera, V., Rasio, F. A., et al. 2008, The Astrophysical Journal Supplement Series, 174, 223

Bhatti, W., Bouma, L. G., & Wallace, J. 2018, `astrobase`

Bonomo, A. S., Desidera, S., Benatti, S., et al. 2017, Astronomy and Astrophysics, 602, A107

Borkovits, T., Rappaport, S., Hajdu, T., & Sztakovics, J. 2015, Monthly Notices of the Royal Astronomical Society, 448, 946

Cáceres, C., Ivanov, V. D., Minniti, D., et al. 2011, Astronomy and Astrophysics, 530, A5

Campo, C. J., Harrington, J., Hardy, R. A., et al. 2011, The Astrophysical Journal, 727, 125

Carter, J. A., Yee, J. C., Eastman, J., Gaudi, B. S., & Winn, J. N. 2008, The Astrophysical Journal, 689, 499

Ciceri, S., Mancini, L., Southworth, J., et al. 2016, Monthly Notices of the Royal Astronomical Society, 456, 990

Collaboration, T. A., Price-Whelan, A. M., Sipöcz, B. M., et al. 2018, arXiv:1801.02634 [astro-ph], arXiv: 1801.02634

Collier Cameron, A., & Jardine, M. 2018, Monthly Notices of the Royal Astronomical Society, 476, 2542

Counselman, C. C. 1973, The Astrophysical Journal, 180, 307

Croll, B., Lafreniere, D., Albert, L., et al. 2011, The Astronomical Journal, 141, 30

Crossfield, I. J. M., Knutson, H., Fortney, J., et al. 2012, The Astrophysical Journal, 752, 81

Dawson, R. I., & Johnson, J. A. 2018, arXiv:1801.06117 [astro-ph], arXiv: 1801.06117

Doyle, A. P., Smalley, B., Maxted, P. F. L., et al. 2013, Monthly Notices of the Royal Astronomical Society, 428, 3164

Dragomir, D., Kane, S. R., Pilyavsky, G., et al. 2011, The Astronomical Journal, 142, 115

Eastman, J., Siverd, R., & Gaudi, B. S. 2010, Publications of the Astronomical Society of the Pacific, 122, 935, arXiv: 1005.4415

Essick, R., & Weinberg, N. N. 2016, The Astrophysical Journal, 816, 18

Foreman-Mackey, D. 2016, The Journal of Open Source Software, 24

Foreman-Mackey, D., Hogg, D. W., Lang, D., & Goodman, J. 2013, Publications of the Astronomical Society of the Pacific, 125, 306

Fukui, A., Narita, N., Tristram, P. J., et al. 2011, Publications of the Astronomical Society of Japan, 63, 287

Gaia Collaboration, Prusti, T., de Bruijne, J. H. J., et al. 2016, Astronomy and Astrophysics, 595, A1

Gaia Collaboration, Brown, A. G. A., Vallenari, A., et al. 2018, Astronomy and Astrophysics, 616, A1

Geller, A. M., Hurley, J. R., & Mathieu, R. D. 2013, The Astronomical Journal, 145, 8

Gibson, N. P., Aigrain, S., Barstow, J. K., et al. 2013, Monthly Notices of the Royal Astronomical Society, 428, 3680

Gillon, M., Anderson, D. R., Triaud, A. H. M. J., et al. 2009a, Astronomy and Astrophysics, 501, 785

Gillon, M., Smalley, B., Hebb, L., et al. 2009b, Astronomy and Astrophysics, 496, 259

Giménez, A., & Bastero, M. 1995, Astrophysics and Space Science, 226, 99

Ginsburg, A., Sipocz, B., Madhura Parikh, et al. 2018, Astropy/Astroquery: V0.3.7 Release

Goldreich, P., & Soter, S. 1966, Icarus, 5, 375

Goodman, J., & Weare, J. 2010, Communications in Applied Mathematics and Computational Science, 5, 65
Hall, D. S. 1989, Space Science Reviews, 50, 219
Hansen, B. M. S. 2010, The Astrophysical Journal, 723, 285
Hebb, L., Collier-Cameron, A., Loeillet, B., et al. 2009, The Astrophysical Journal, 693, 1920
Hellier, C., Anderson, D. R., Collier Cameron, A., et al. 2009, Nature, 460, 1098
Hoyer, S., Rojo, P., & López-Morales, M. 2012, The Astrophysical Journal, 748, 22
Hoyer, S., López-Morales, M., Rojo, P., et al. 2013, Monthly Notices of the Royal Astronomical Society, 434, 46
Huitson, C. M., Désert, J.-M., Bean, J. L., et al. 2017, The Astronomical Journal, 154, 95
Hunter, J. D. 2007, Computing in Science & Engineering, 9, 90
Husnoo, N., Pont, F., Mazeh, T., et al. 2012, Monthly Notices of the Royal Astronomical Society, 422, 3151
Hut, P. 1980, Astronomy and Astrophysics, 92, 167
Ibgui, L., Burrows, A., & Spiegel, D. S. 2010, The Astrophysical Journal, 713, 751
Jackson, B., Barnes, R., & Greenberg, R. 2009, The Astrophysical Journal, 698, 1357
Jackson, B., Jensen, E., Peacock, S., Arras, P., & Penev, K. 2016, Celestial Mechanics and Dynamical Astronomy, 1
Jenkins, J. M., Twicken, J. D., McCauliff, S., et al. 2016, Software and Cyberinfrastructure for Astronomy IV, 9913, 99133E
Jones, E., Oliphant, T., Peterson, P., et al. 2001, Open source scientific tools for Python
Jordán, A., Espinoza, N., Rabus, M., et al. 2013, The Astrophysical Journal, 778, 184
Kass, R. E., & Raftery, A. E. 1995, Journal of the American Statistical Association, 90, 773
Knutson, H. A., Charbonneau, D., Allen, L. E., et al. 2007, Nature, 447, 183
Knutson, H. A., Fulton, B. J., Montet, B. T., et al. 2014, The Astrophysical Journal, 785, 126
Kostov, V. B., McCullough, P. R., Carter, J. A., et al. 2014, The Astrophysical Journal, 784, 14
Kovács, G., Zucker, S., & Mazeh, T. 2002, Astronomy and Astrophysics, 391, 369
Kozai, Y. 1962, The Astronomical Journal, 67, 591
Kreidberg, L. 2015, Publications of the Astronomical Society of the Pacific, 127, 1161
Lainey, V., Arlot, J.-E., Karatekin, Ã., & van Hoolst, T. 2009, Nature, 459, 957
Levrard, B., Winisdoerffer, C., & Chabrier, G. 2009, The Astrophysical Journal, 692, L9
Lidov, M. L. 1962, Planetary and Space Science, 9, 719
López-Morales, M., Coughlin, J. L., Sing, D. K., et al. 2010, The Astrophysical Journal, 716, L36
Maciejewski, G., Dimitrov, D., FernÃąndez, M., et al. 2016, Astronomy and Astrophysics, 588, L6
MacLeod, M., Cantiello, M., & Soares-Furtado, M. 2018, The Astrophysical Journal Letters, 853, L1
Mandel, K., & Agol, E. 2002, The Astrophysical Journal, 580, L171, arXiv: astro-ph/0210099
Mansouri-Samani, M., et al. 2018, TESS Science Data Products Description Document, EXP-TESS-ARC-ICD-0014, https://archive.stsci.edu/missions/tess/doc/EXP-TESS-ARC-ICD-TM-0014.pdf
Mardling, R. A. 2007, Monthly Notices of the Royal Astronomical Society, 382, 1768
Masuda, K. 2015, The Astrophysical Journal, 805, 28
—. 2017, The Astronomical Journal, 154, 64
Matsakos, T., & Königl, A. 2016, The Astrophysical Journal Letters, 820, L8
Matsumura, S., Peale, S. J., & Rasio, F. A. 2010, The Astrophysical Journal, 725, 1995
Maxted, P. F. L., Anderson, D. R., Doyle, A. P., et al. 2013, Monthly Notices of the Royal Astronomical Society, 428, 2645
McKinney, W. 2010, in Proceedings of the 9th Python in Science Conference, ed. S. van der Walt & J. Millman, 51
Meibom, S., & Mathieu, R. D. 2005, The Astrophysical Journal, 620, 970
Metzger, B. D., Giannios, D., & Spiegel, D. S. 2012, Monthly Notices of the Royal Astronomical Society, 425, 2778
Millholland, S., & Laughlin, G. 2018, arXiv:1812.01624 [astro-ph], arXiv: 1812.01624
Milliman, K. E., Mathieu, R. D., Geller, A. M., et al. 2014, The Astronomical Journal, 148, 38
Mills, S. M., & Fabrycky, D. C. 2017, The Astronomical Journal, 153, 45
Moyano, M., Almeida, L. A., von Essen, C., Jablonski, F., & Pereira, M. G. 2017, Monthly Notices of the Royal Astronomical Society, 471, 650
Ni, D. 2018, Astronomy & Astrophysics, 613, A32
Nikolov, N., Henning, T., Koppenhoefer, J., et al. 2012, Astronomy and Astrophysics, 539, A159
Nikolov, N., Sing, D. K., Burrows, A. S., et al. 2015, Monthly Notices of the Royal Astronomical Society, 447, 463
Ogilvie, G. I. 2014, Annual Review of Astronomy and Astrophysics, 52, 171, arXiv: 1406.2207
Patra, K. C., Winn, J. N., Holman, M. J., et al. 2017, The Astronomical Journal, 154, 4
Pedregosa, F., Varoquaux, G., Gramfort, A., et al. 2011, Journal of Machine Learning Research, 12, 2825
Penev, K., Bouma, L. G., Winn, J. N., & Hartman, J. D. 2018, The Astronomical Journal, 155, 165
Penev, K., Jackson, B., Spada, F., & Thom, N. 2012, The Astrophysical Journal, 751, 96

Penev, K., & Sasselov, D. 2011, The Astrophysical Journal, 731, 67
Penev, K., Hartman, J. D., Bakos, G. Ã., et al. 2016, The Astronomical Journal, 152, 127
Pérez, F., & Granger, B. E. 2007, Computing in Science and Engineering, 9, 21
Petrucci, R., Jofré, E., Ferrero, L. V., et al. 2018, Monthly Notices of the Royal Astronomical Society, 473, 5126
Petrucci, R., Jofré, E., Schwartz, M., et al. 2013, The Astrophysical Journal Letters, 779, L23
Phinney, E. S. 1992, Philosophical Transactions of the Royal Society of London Series A, 341, 39
Pont, F. 2009, Monthly Notices of the Royal Astronomical Society, 396, 1789
Pont, F., Husnoo, N., Mazeh, T., & Fabrycky, D. 2011, Monthly Notices of the Royal Astronomical Society, 414, 1278
Rafikov, R. R. 2009, The Astrophysical Journal, 700, 965
Ragozzine, D., & Wolf, A. S. 2009, The Astrophysical Journal, 698, 1778, arXiv: 0807.2856
Ranjan, S., Charbonneau, D., Désert, J.-M., et al. 2014, The Astrophysical Journal, 785, 148
Rasio, F. A., Tout, C. A., Lubow, S. H., & Livio, M. 1996, The Astrophysical Journal, 470, 1187
Ricker, G., & Vanderspek, R. 2018, Data Products From TESS Data Alerts, https://archive.stsci.edu/prepds/tess-data-alerts/index.html
Ricker, G. R., Winn, J. N., Vanderspek, R., et al. 2015, Journal of Astronomical Telescopes, Instruments, and Systems, 1, 014003
Sada, P. V., Deming, D., Jennings, D. E., et al. 2012, Publications of the Astronomical Society of the Pacific, 124, 212
Sanchis-Ojeda, R., Winn, J. N., Holman, M. J., et al. 2011, The Astrophysical Journal, 733, 127
Schwarzschild, M. 1958, Structure and evolution of the stars (Princeton Univesity Press), Ch. 18
Seager, S., & Mallén-Ornelas, G. 2003, The Astrophysical Journal, 585, 1038
Shklovskii, I. S. 1970, Soviet Astronomy, 13, 562
Smith, J. C., Morris, R. L., Jenkins, J. M., et al. 2017a, Kepler Science Document, 7
Smith, J. C., Stumpe, M. C., Jenkins, J. M., et al. 2017b, Kepler Science Document, 8
Söderhjelm, S. 1980, Astronomy and Astrophysics, 89, 100
Southworth, J. 2011, Monthly Notices of the Royal Astronomical Society, 417, 2166
Southworth, J., Hinse, T. C., Jørgensen, U. G., et al. 2009, Monthly Notices of the Royal Astronomical Society, 396, 1023
Stassun, K. G., Collins, K. A., & Gaudi, B. S. 2017, The Astronomical Journal, 153, 136
Stassun, K. G., & Torres, G. 2018, The Astrophysical Journal, 862, 61
Stassun, K. G., Oelkers, R. J., Pepper, J., et al. 2018, The Astronomical Journal, 156, 102
Sullivan, P. W., et al. 2015, ApJ, 809, 77
Szabó, G. M., Pál, A., Derekas, A., et al. 2012, Monthly Notices of the Royal Astronomical Society, 421, L122
Szabó, G. M., Simon, A., & Kiss, L. L. 2014, Monthly Notices of the Royal Astronomical Society, 437, 1045
Thompson, S., et al. 2013, Kepler Data Release 19 Notes Q14, KSCI-19059-001, https://archive.stsci.edu/kepler/release_notes/release_notes19/DataRelease_19_20130204.pdf
Torres, G., Andersen, J., & Giménez, A. 2010, Astronomy and Astrophysics Review, 18, 67
Tregloan-Reed, J., Southworth, J., Burgdorf, M., et al. 2015, Monthly Notices of the Royal Astronomical Society, 450, 1760
Triaud, A. H. M. J., Collier Cameron, A., Queloz, D., et al. 2010, Astronomy and Astrophysics, 524, A25
Urban, S., & Seidelmann, P. 2012, Explanatory Supplement to the Astronomical Almanac (University Science Books)
Valsecchi, F., Rappaport, S., Rasio, F. A., Marchant, P., & Rogers, L. A. 2015, The Astrophysical Journal, 813, 101
Wahl, S. M., Hubbard, W. B., & Militzer, B. 2016, The Astrophysical Journal, 831, 14
Walt, S. v. d., Colbert, S. C., & Varoquaux, G. 2011, Computing in Science & Engineering, 13, 22
Watson, C. A., & Marsh, T. R. 2010, Monthly Notices of the Royal Astronomical Society, 405, 2037
Weinberg, N. N., Sun, M., Arras, P., & Essick, R. 2017, The Astrophysical Journal Letters, 849, L11
Welsh, W. F., Orosz, J. A., Short, D. R., et al. 2015, The Astrophysical Journal, 809, 26
Wilkins, A. N., Delrez, L., Barker, A. J., et al. 2017, The Astrophysical Journal Letters, 836, L24
Williams, P. K. G., Charbonneau, D., Cooper, C. S., Showman, A. P., & Fortney, J. J. 2006, The Astrophysical Journal, 649, 1020
Wilson, D. M., Gillon, M., Hellier, C., et al. 2008, The Astrophysical Journal Letters, 675, L113
Winn, J. N. 2010, Exoplanets, 55
—. 2013, TESS Science Memo No. 1, Version 2. Available upon request.
Winn, J. N., Holman, M. J., Carter, J. A., et al. 2009, The Astronomical Journal, 137, 3826
Winn, J. N., Noyes, R. W., Holman, M. J., et al. 2005, The Astrophysical Journal, 631, 1215
Zahn, J.-P. 1977, Astronomy and Astrophysics, 500, 121
Zhou, G., Bayliss, D. D. R., Kedziora-Chudczer, L., et al. 2015, Monthly Notices of the Royal Astronomical Society, 454, 3002

APPENDIX

A. VERIFYING THE TESS TIME STAMPS

Any systematic offset between the TESS times and the true barycentric reference would cast doubt on the results of this study. There is historic precedent: Kepler had a systematic error in its timestamps that was corrected only in Q14 (Thompson et al. 2013, Section 3.4).

We devised two checks on the absolute calibration of the TESS time system. First, in § A.1, we recalculate and confirm the barycentric correction reported by SPOC in the TESS lightcurve file headers. In § A.2, we measure the transit times of other hot Jupiters, and use them to rule out a global TESS time offset larger than about a minute. The latter test confirms that WASP-4b is an outlier.

A.1. *Using the headers of the lightcurve files*

The TESS lightcurve files provide observation start and end times in three different time systems: $\mathrm{JD_{UTC}}$, $\mathrm{JD_{TDB}}$, and $\mathrm{BJD_{TDB}}$. First, we verified for a few select lightcurve files that $\mathrm{JD_{UTC}}$ lagged behind $\mathrm{JD_{TDB}}$ by the expected $32.184+N$ seconds, where N is the number of leap-seconds since 1961. For the relevant observation time, $N = 37$, and the offset was as expected. Then, using the $\mathrm{JD_{UTC}}$ timestamp, we recalculated the barycentric correction computed by SPOC, using the Eastman et al. 2010 calculator. Due to the first author's ignorance of the spacecraft position, we assumed that the observer was located at the Earth's geocenter, and used the correct direction for each star. This gave us times in $\mathrm{BJD_{TDB}}$ that agreed with the archival times to within 1.7 seconds. This offset is comparable to the light-travel delay expected for TESS on its orbit from perigee of $\approx 20R_\oplus$ to apogee of $\approx 60R_\oplus$.

This calculation bounds any error in the SPOC barycentric julian date correction to be less than 1.7 seconds. This is smaller than the effect of interest, so we treat the SPOC BJD correction as "verified", and proceed to a subsequent test.

A.2. *Using other hot Jupiters as references*

If the observed timing delay in WASP-4b were caused by a systematic offset between the TESS times and the $\mathrm{BJD_{TDB}}$ reference, we might expect that it would apply to other hot Jupiters as well. This test can rule out an important class of clock error – a systematic global offset.

To explore this possibility, we repeat the timing analysis of the main paper, for other hot Jupiters with long preceding observing baselines. We first checked which hot Jupiters were observed over the first two TESS sectors using a combination of `tessmaps`[7] and TEPCat (Southworth 2011). We then selected hot Jupiters for which there were at least five distinct epochs reported in the peer-reviewed literature. We required that each observation be of a single transit, that the midpoint be fit as a free parameter, and that the time system be clearly documented. Our final hot Jupiter sample included WASPs-4b, -5b, -6b, -18b, and -46b. The collected and measured times are given in Tables 5, 6, 7, and 8 for each.

Using the literature timing data for each hot Jupiter, we then performed a least-squares fit to a linear ephemeris. Using the best-fit values and variances, we calculated the uncertainty on the predicted transit time during the TESS observations. This gave 9, 94, 18, 42, and 60 seconds for WASPs-4b, -5b, -6b, -18b, and -46b. We show in Figure 6 that WASP-4b is the only hot Jupiter that transited significantly earlier than expected.

To convert this intuition into a quantitative limit, for each hot Jupiter we considered the model

$$t_{\mathrm{tra}}(E) = t_0 + PE + t_{\mathrm{offset}}, \tag{A1}$$

for t_{offset} a systematic constant offset between the reported timestamps and the true $\mathrm{BJD_{TDB}}$ reference. Our priors were

$$t_0 \sim \mathcal{N}[t_0', \sigma_{t_0'}], \tag{A2}$$

$$P \sim \mathcal{N}[P', \sigma_{P'}], \tag{A3}$$

$$t_{\mathrm{offset}} \sim \mathcal{U}[-20\sigma_{t_0'}, 20\sigma_{t_0'}], \tag{A4}$$

where $\mathcal{N}$ and $\mathcal{U}$ denote a normal and uniform distribution, (t_0', P') are the best-fit reference time and period using only the literature transit times, and $(\sigma_{t_0'}, \sigma_{P'})$ are their uncertainties.

For each planet, we then ask: what fraction of the posterior for t_{offset} is consistent with an offset worse than 77 seconds? For WASP-4b, the answer is unsurpringly about half. For WASP-6b, the most constraining object, about 1 sample in 2 million is consistent with such a timing offset (4.9σ). For WASP-18b, 1 in 63 samples would be consistent with this timing offset (2.1σ), and in WASP-46b, the limit is 1 in 38 samples (1.9σ). For WASP-5b, the predicted time is too imprecise to rule out timing offsets at the necessary amplitude. Multiplying the three independent probabilities for WASPs-5b, 6b, and -18b, we rule out $t_{\mathrm{offset}} < -77$ seconds at 6.3σ, or about about 1 part in 5 billion.

[7] github.com/lgbouma/tessmaps

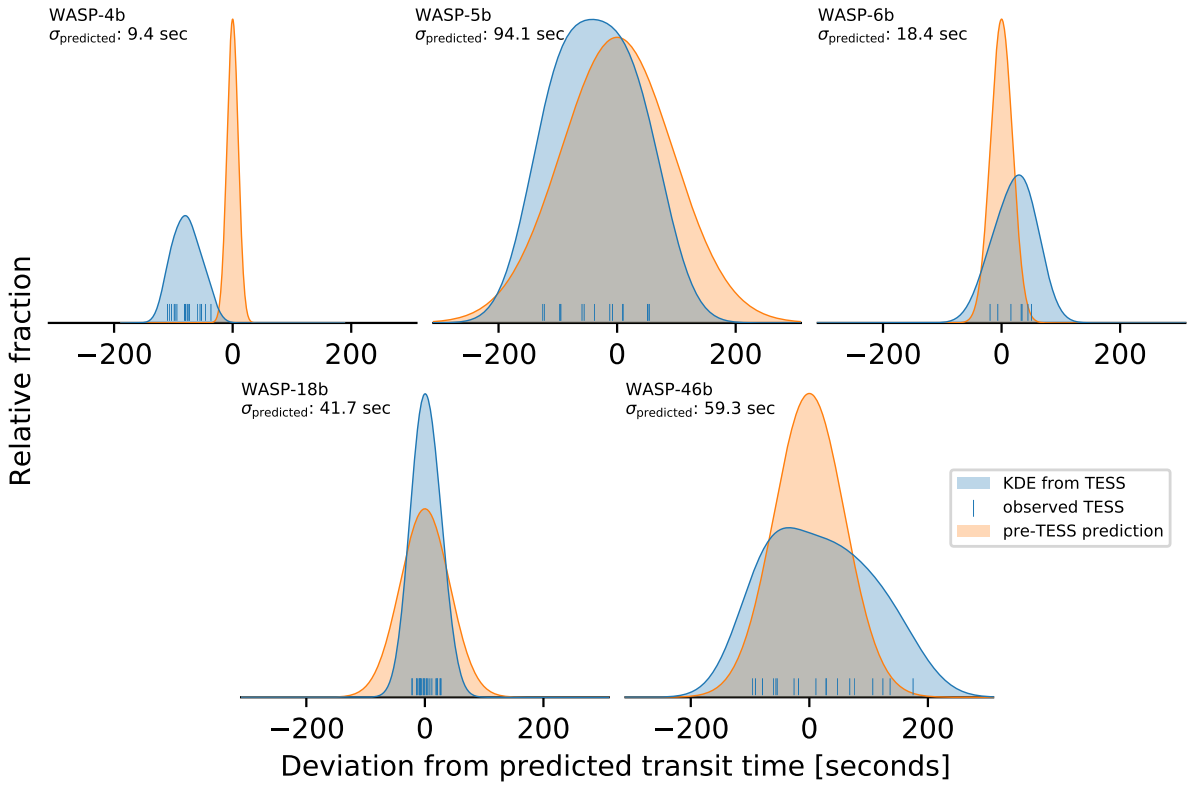

Figure 6. There is no evidence for a systematic offset between TESS times and the barycentric reference. While the WASP-4b transits fell about 75 seconds earlier than predicted, other well-observed hot Jupiters, in particular WASP-6b and WASP-18b, arrived on time. Ticks are observed TESS transit midtimes; the blue distribution is a kernel density estimate; the orange distribution is a gaussian centered on zero using the indicated 1σ standard deviation from the pre-TESS prediction.

Table 5. WASP-5b transit times, uncertainties, and references.

t_{tra} [BJD_{TDB}]	$\sigma_{t_{tra}}$ [days]	Epoch	Reference
2454383.76750	0.00040	-885	Anderson et al. (2008)
2454387.02275	0.00100	-883	Anderson et al. (2008)
2454636.17459	0.00082	-730	Fukui et al. (2011)
2454699.68303	0.00041	-691	Hoyer et al. (2012)
2454707.82465	0.00052	-686	Hoyer et al. (2012)
2454707.82523	0.00025	-686	Southworth et al. (2009)
2454730.62243	0.00031	-672	Southworth et al. (2009)
2454730.62301	0.00076	-672	Hoyer et al. (2012)
2454761.56356	0.00047	-653	Hoyer et al. (2012)
2454772.96212	0.00075	-646	Fukui et al. (2011)
2454774.59093	0.00030	-645	Hoyer et al. (2012)
2454787.61792	0.00069	-637	Hoyer et al. (2012)
2455005.82714	0.00036	-503	Hoyer et al. (2012)
2455049.79540	0.00080	-476	Hoyer et al. (2012)
2455075.84947	0.00056	-460	Dragomir et al. (2011)
2455079.10830	0.00079	-458	Fukui et al. (2011)

Table 5 continued

Table 5 *(continued)*

t_{tra} [BJD$_{TDB}$]	$\sigma_{t_{tra}}$ [days]	Epoch	Reference
2455110.04607	0.00089	-439	Fukui et al. (2011)
2455123.07611	0.00079	-431	Fukui et al. (2011)
2455129.58759	0.00043	-427	Hoyer et al. (2012)
2455364.08150	0.00110	-283	Fukui et al. (2011)
2455377.10955	0.00093	-275	Fukui et al. (2011)
2455448.75927	0.00110	-231	Dragomir et al. (2011)
2456150.61479	0.00056	200	Moyano et al. (2017)
2456150.61396	0.00057	200	Moyano et al. (2017)
2458355.50829	0.00083	1554	This work
2458357.13741	0.00071	1555	This work
2458358.76412	0.00068	1556	This work
2458360.39377	0.00070	1557	This work
2458362.02273	0.00073	1558	This work
2458363.64908	0.00090	1559	This work
2458365.27827	0.00071	1560	This work
2458366.90627	0.00075	1561	This work
2458370.16411	0.00076	1563	This work
2458371.79126	0.00071	1564	This work
2458373.42123	0.00075	1565	This work
2458375.04910	0.00069	1566	This work
2458376.67856	0.00074	1567	This work
2458378.30530	0.00087	1568	This work
2458379.93419	0.00082	1569	This work

NOTE— t_{tra} is the measured transit midtime, and $\sigma_{t_{tra}}$ is its 1σ uncertainty. The "Reference" column refers to the work describing the original observations. All the literature times except for the two Moyano et al. (2017) times are from the homogeneous Hoyer et al. (2012) analysis.

Table 6. WASP-6b transit times, uncertainties, and references.

t_{tra} [BJD$_{TDB}$]	$\sigma_{t_{tra}}$ [days]	Epoch	Reference
2454425.02167	0.00022	-398	Gillon et al. (2009a)
2455009.83622	0.00021	-224	Tregloan-Reed et al. (2015)
2455046.80720	0.00015	-213	Tregloan-Reed et al. (2015)
2455073.69529	0.00013	-205	Tregloan-Reed et al. (2015)
2455409.79541	0.00010	-105	Tregloan-Reed et al. (2015)
2455446.76621	0.00058	-94	Dragomir et al. (2011)
2455473.65439	0.00097	-86	Jordán et al. (2013)
2455846.72540	0.00045	25	Sada et al. (2012)
2456088.71801	0.00013	97	Nikolov et al. (2015)
2456095.43974	0.00017	99	Nikolov et al. (2015)
2456132.41082	0.00017	110	Nikolov et al. (2015)
2458357.39410	0.00033	772	This work
2458360.75573	0.00033	773	This work
2458364.11691	0.00032	774	This work
2458370.83872	0.00033	776	This work
2458374.19952	0.00031	777	This work
2458377.56026	0.00033	778	This work
2458380.92185	0.00038	779	This work

NOTE— t_{tra} is the measured transit midtime, and $\sigma_{t_{tra}}$ is its 1σ uncertainty. The "Reference" column refers to the work describing the original observations.

Table 7. WASP-18b transit times, uncertainties, and references.

t_{tra} [BJD$_{TDB}$]	$\sigma_{t_{tra}}$ [days]	Epoch	Reference
2454221.48163	0.00038	-3730	Hellier et al. (2009)
2455221.30420	0.00010	-2668	Maxted et al. (2013)
2455432.18970	0.00010	-2444	Maxted et al. (2013)
2455470.78850	0.00040	-2403	Maxted et al. (2013)
2455473.61440	0.00090	-2400	Maxted et al. (2013)
2455554.57860	0.00050	-2314	Maxted et al. (2013)
2455570.58400	0.00048	-2297	Maxted et al. (2013)
2455876.55590	0.00130	-1972	Maxted et al. (2013)
2456896.14780	0.00080	-889	Wilkins et al. (2017)
2457255.78320	0.00030	-507	Wilkins et al. (2017)
2457319.80100	0.00039	-439	Wilkins et al. (2017)
2458354.45778	0.00015	660	This work
2458355.39934	0.00015	661	This work
2458356.34073	0.00016	662	This work
2458357.28228	0.00017	663	This work
2458358.22348	0.00017	664	This work
2458359.16512	0.00016	665	This work
2458360.10662	0.00016	666	This work
2458361.04813	0.00017	667	This work

Table 7 continued

Table 7 *(continued)*

t_{tra} [BJD$_{TDB}$]	$\sigma_{t_{tra}}$ [days]	Epoch	Reference
2458361.98968	0.00016	668	This work
2458362.93129	0.00016	669	This work
2458363.87266	0.00018	670	This work
2458364.81373	0.00016	671	This work
2458365.75526	0.00017	672	This work
2458366.69704	0.00019	673	This work
2458367.63835	0.00187	674	This work
2458369.52126	0.00017	676	This work
2458370.46285	0.00017	677	This work
2458371.40405	0.00016	678	This work
2458372.34536	0.00017	679	This work
2458373.28727	0.00017	680	This work
2458374.22817	0.00016	681	This work
2458375.16976	0.00016	682	This work
2458376.11124	0.00017	683	This work
2458377.05269	0.00016	684	This work
2458377.99448	0.00017	685	This work
2458378.93572	0.00016	686	This work
2458379.87720	0.00016	687	This work
2458380.81891	0.00017	688	This work

NOTE— t_{tra} is the measured transit midtime, and $\sigma_{t_{tra}}$ is its 1σ uncertainty. The "Reference" column refers to the work describing the original observations. All the literature times are from the homogeneous Wilkins et al. (2017) analysis.

Table 8. WASP-46b transit times, uncertainties, and references.

t_{tra} [BJD$_{TDB}$]	$\sigma_{t_{tra}}$ [days]	Epoch	Reference
2455396.60785	0.00062	-673	Anderson et al. (2012)
2455449.53082	0.00026	-636	Anderson et al. (2012)
2455722.73178	0.00023	-445	Ciceri et al. (2016)
2455757.06195	0.00094	-421	Petrucci et al. (2018)
2455858.61833	0.00009	-350	Ciceri et al. (2016)
2456108.92771	0.00094	-175	Petrucci et al. (2018)
2456111.79422	0.00016	-173	Ciceri et al. (2016)
2456111.79413	0.00012	-173	Ciceri et al. (2016)
2456111.79424	0.00015	-173	Ciceri et al. (2016)
2456130.38895	0.00042	-160	Petrucci et al. (2018)
2456131.81456	0.00112	-159	Petrucci et al. (2018)
2456194.75916	0.00027	-115	Ciceri et al. (2016)
2456217.64127	0.00015	-99	Ciceri et al. (2016)
2456217.64156	0.00013	-99	Ciceri et al. (2016)
2456227.65574	0.00060	-92	Petrucci et al. (2018)
2456407.88096	0.00015	34	Ciceri et al. (2016)
2456407.88085	0.00018	34	Ciceri et al. (2016)
2456407.88148	0.00028	34	Ciceri et al. (2016)
2456407.88159	0.00043	34	Ciceri et al. (2016)
2456460.80526	0.00017	71	Ciceri et al. (2016)
2456460.80450	0.00024	71	Ciceri et al. (2016)
2456460.80547	0.00064	71	Ciceri et al. (2016)
2456510.86818	0.00060	106	Petrucci et al. (2018)

Table 8 continued

Table 8 *(continued)*

t_{tra} [BJD$_{TDB}$]	$\sigma_{t_{tra}}$ [days]	Epoch	Reference
2456510.86699	0.00015	106	Petrucci et al. (2018)
2456516.58667	0.00119	110	Petrucci et al. (2018)
2456520.88012	0.00064	113	Petrucci et al. (2018)
2456533.75260	0.00071	122	Ciceri et al. (2016)
2456533.75480	0.00015	122	Ciceri et al. (2016)
2456576.66289	0.00109	152	Petrucci et al. (2018)
2456589.54197	0.00090	161	Petrucci et al. (2018)
2456609.56653	0.00043	175	Petrucci et al. (2018)
2456839.85440	0.00123	336	Petrucci et al. (2018)
2456862.74085	0.00048	352	Petrucci et al. (2018)
2456882.76566	0.00073	366	Petrucci et al. (2018)
2456885.62429	0.00053	368	Petrucci et al. (2018)
2456915.66040	0.00123	389	Petrucci et al. (2018)
2456942.83880	0.00078	408	Petrucci et al. (2018)
2456948.56384	0.00074	412	Petrucci et al. (2018)
2457274.68458	0.00184	640	Petrucci et al. (2018)
2457294.70886	0.00140	654	Petrucci et al. (2018)
2457550.74797	0.00031	833	Petrucci et al. (2018)
2457593.65692	0.00024	863	Petrucci et al. (2018)
2457600.80985	0.00039	868	Petrucci et al. (2018)
2457610.82286	0.00020	875	Petrucci et al. (2018)
2458326.00972	0.00091	1375	This work
2458327.43899	0.00093	1376	This work
2458328.86970	0.00094	1377	This work
2458330.29965	0.00105	1378	This work
2458331.73234	0.00105	1379	This work
2458333.15977	0.00086	1380	This work
2458334.59230	0.00095	1381	This work
2458336.02222	0.00082	1382	This work
2458337.45111	0.00099	1383	This work
2458340.31143	0.00093	1385	This work
2458341.74347	0.00093	1386	This work
2458343.17362	0.00093	1387	This work
2458344.60303	0.00110	1388	This work
2458346.03436	0.00091	1389	This work
2458347.46335	0.00168	1390	This work
2458348.89621	0.00086	1391	This work
2458350.32672	0.00101	1392	This work
2458351.75486	0.00103	1393	This work

NOTE— t_{tra} is the measured transit midtime, and $\sigma_{t_{tra}}$ is its 1σ uncertainty. The "Reference" column refers to the work describing the original observations. All the literature times are from the homogeneous Petrucci et al. (2018) analysis. 14 of the lightcurves were acquired by ETD observers (see Petrucci et al. 2018).